

Spin-wave dynamics controlled by tunable ac magnonic crystal

Ankang Liu¹ and Alexander M. Finkel'stein^{1,2}

¹Department of Physics and Astronomy, Texas A&M University, College Station, Texas 77843-4242, USA

²Department of Condensed Matter Physics, The Weizmann Institute of Science, Rehovot 76100, Israel

The magnonic crystal, which has a spatial modulation wave vector q , couples the spin wave with wave vector k to the one with wave vector $k - q$. For a conventional magnonic crystal with direct current (dc) supply, the spin waves around $q/2$ are resonantly coupled to the waves near $-q/2$, and a band gap is opened at $k = \pm q/2$. If instead of the dc current the magnonic crystal is supplied with an alternating current (ac), then the band gap is *shifted* to k satisfying $|\omega_s(k) - \omega_s(k - q)| = \omega_{ac}$; here $\omega_s(k)$ is the dispersion of the spin wave, while ω_{ac} is the frequency of the ac modulation. The resulting gap in the case of the ac magnonic crystal is the half of the one caused by the dc with the same amplitude of modulation. The time evolution of the resonantly coupled spin waves controlled by properly suited ac pulses can be well interpreted as the motion on a Bloch sphere. The tunability of the ac magnonic crystal broadens the perspective of spin-wave computing.

Introduction. Interference of classical waves can be exploited for building computing devices that may work faster than the classical ones for certain tasks [1–5]. As it was demonstrated in Ref. [6], a computing machine relying on the spin-wave interference outperforms a classical digital computer on a database search. In that work, the authors utilized a linear superposition of two spin waves with different phases to encode a “qubit” state, with each “qubit” sent through its own waveguide and controlled by an individual phase shifter. However, scaling up such a spin-wave computing device will be a significant challenge. To address this challenge, in this paper we explore the possibilities of using a single *tunable* ac magnonic crystal for the control of different spin-wave pairs.

Spin waves are the collective wave excitations in the magnetically ordered system, which have the frequencies typically ranged from GHz up to even THz. The utilization of spin waves for the purposes of quantum-information exchange was proposed long ago [7]. The later studies [8, 9] showed that the spin waves excited in yttrium iron garnet (YIG) can have both lifetime and coherence time longer than 100 ns. In addition, the ability of exciting exchange spin waves with wavelengths down to the nanometer range [10, 11] allows one to build compact spin-wave-based devices at the submicron scale. All these properties make the low-damping coherent spin waves a suitable candidate for performing rapid data processing and wave computing [12–17].

As an efficient way to control spin waves, magnonic crystals have been studied both experimentally and theoretically [18–22]. A prototypical current-induced magnonic crystal for ferromagnet is schematically depicted in Fig. 1(a) (cf. Refs. [18, 19]). If a dc current, $I(t) = I_0$, is supplied through a metallic meander structure with a period d , a spatially modulated static magnetic field generates a magnonic crystal for the spin waves propagating along the direction of the modulation. For the spin waves with a symmetric spectrum, the dc magnonic crystal resonantly couples the spin waves with wave vectors around $\pm q/2$, where $q = 2\pi/d$ is determined by the period of the spatial modulation. As shown in Fig. 1(b), the coupling of the two degenerate waves opens a

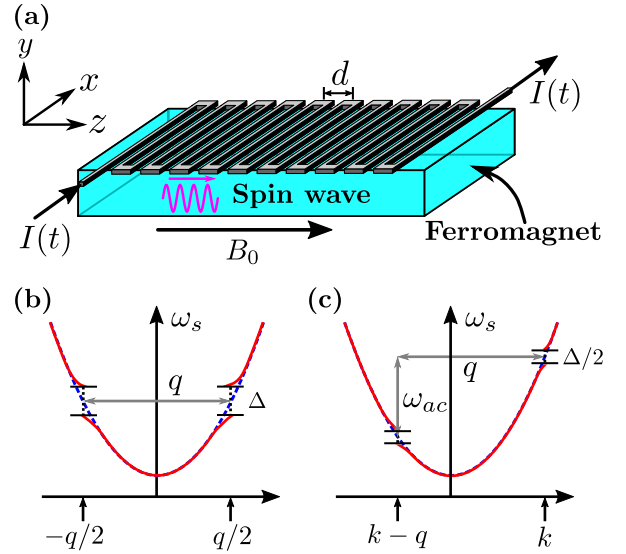


FIG. 1. (a) A schematic setup of the current-induced magnonic crystal, which was used for studying the spin-wave dynamics in experiments [18, 19]. The meander structure at the top of the ferromagnet creates a spatially modulated magnetic field, which is $\propto I(t) \cos(qz) \mathbf{e}_z$, along the z direction. Here, $q = 2\pi/d$. In the second row, we sketch the spin-wave spectrum when the magnonic crystal is switched on (the solid red curves) and when it is not effective (the dashed blue curves). Panel (b) is for the dc magnonic crystal while (c) is for the ac case (the gaps around the wave vectors $q - k$ and $-k$ are not shown). The band gap $\Delta \propto I_0$. Note that the band gap caused by the ac magnonic crystal is the half of the one created by the dc with the same amplitude I_0 .

band gap Δ , which is $\propto I_0$ [18, 19]. In practice, for an incident spin-wave packet, after switching on the dc magnonic crystal, the spin-wave components that are under the resonant scattering conditions start to alternate between the forward- and backward-propagating states; while the out-of-resonance spectral components are unaffected by the perturbation and propagate unidirectionally.

In this paper, we consider the same experimental setup

as was exploited in Refs. [18, 19], but extend the discussion to an ac modulated magnonic crystal, i.e., when the current $I(t) = I_0 \cos(\omega_{ac}t + \varphi_{ac})$. We show that under the limit $\omega_{ac} \gg \Delta$ a spin-wave pair with wave vectors k and $k - q$ can be controlled by a *tunable* ac magnonic crystal that satisfies the *shifted resonance* condition $|\omega_s(k) - \omega_s(k - q)| = \omega_{ac}$ [cf. Fig. 1(c)].

Spin-wave scattering induced by magnonic crystal. Suppose that, initially (i.e., at $t < 0$), there was a free spin wave with wave vector $\mathbf{k} = k\mathbf{e}_z$ propagating inside the magnet. We consider a device fabricated from a ferromagnet with all spins located on a cubic lattice. To present the idea we will restrict ourselves to the spin-wave excitations originating from the short-range exchange couplings. This is sufficient for illustrating the concept of the shifted resonance. Note that the scheme proposed in this paper is general and applicable to all types of spin waves (e.g., the dipolar spin-wave modes). In the continuum limit, the spin operators become a space- and time-dependent variable $\mathbf{S}(\mathbf{r}, t)$ (see Supplemental Material (SM) [23] for the details). Before the magnonic crystal is switched on, the constant external magnetic field $\mathbf{B} = B_0\mathbf{e}_z$ aligns all spins along the z direction in the ground state. In the case of a spin-wave excitation, $\mathbf{S}(\mathbf{r}, t)$ deviates from the equilibrium and acquires small $S^{x,y}(\mathbf{r}, t)$. The linearized equation in $S^{x,y}(\mathbf{r}, t)$ can be solved by a plane wave $S^+(\mathbf{r}, t) \equiv S^x(\mathbf{r}, t) + iS^y(\mathbf{r}, t) = (\Delta S)e^{i[\mathbf{k}\cdot\mathbf{r} - \omega_s(\mathbf{k})t + \varphi_s]}$ [23], where ΔS is the amplitude of the spin wave, φ_s is its initial phase, and $\omega_s(\mathbf{k}) = Ak^2 + \gamma B_0$ gives the spin-wave dispersion. Here, $A > 0$ is determined by the ferromagnetic exchange coupling between the nearest neighboring spins and γ is the gyromagnetic ratio of the spin.

Next, at $t = 0$, one switches on the ac modulated magnonic crystal, which for $t > 0$ is described by $\Delta B_0 \cos(\omega_{ac}t + \varphi_{ac}) \cos(qz)\mathbf{e}_z$. Here, ΔB_0 is the intensity of the magnonic crystal controlled by I_0 , the frequency of the ac modulation is given by ω_{ac} , while φ_{ac} is the initial phase determined at the moment $t = 0$. In the discussed geometry, the spin-wave propagation is effectively one-dimensional. To find what will be the dynamics of the spin wave after $t = 0$, one needs to solve $S^+(z, t)$ from the equation [23]

$$\frac{dS^+}{dt} = iA\nabla^2 S^+ - i\gamma[B_0 + \Delta B_0 \cos(\omega_{ac}t + \varphi_{ac}) \cos(qz)]S^+, \quad (1)$$

by matching the solution for $t > 0$ with the free spin-wave solution for $t < 0$.

The magnonic crystal term in Eq. (1) couples the spin-wave state k to the state $k - q$ as long as $|\omega_s(k) - \omega_s(k - q)| \approx \omega_{ac}$. To better understand the spin-wave dynamics under the ac magnonic crystal, we look for the solution of Eq. (1) in the form

$$S^+(z, t) = (\Delta S) [\mathcal{S}_p(t) \sin(k_+z) + \mathcal{S}_m(t) \sin(k_-z) + \mathcal{C}_p(t) \cos(k_+z) + \mathcal{C}_m(t) \cos(k_-z)]. \quad (2)$$

Here, we introduced four complex time-dependent coefficients $\mathcal{S}_{p/m}(t)$ and $\mathcal{C}_{p/m}(t)$ in front of the basis functions $\sin(k_{\pm}z)$ and $\cos(k_{\pm}z)$, respectively. Solution (2) describes the mutual scatterings between a pair of the spin waves with the wave vectors $k = k_+ = q/2 + \delta k$ and $k - q = -k_- = -q/2 + \delta k$. Although the scattering occurs between the spin waves with the oppositely directed wave vectors, the wave vectors k_{\pm} are defined here as their absolute values and, therefore, are positive (we assume that $-q/2 < \delta k < q/2$). Note that, in Eq. (2), the contributions from the spin waves with wave vectors $\pm 3q/2 + \delta k$ and higher are neglected.

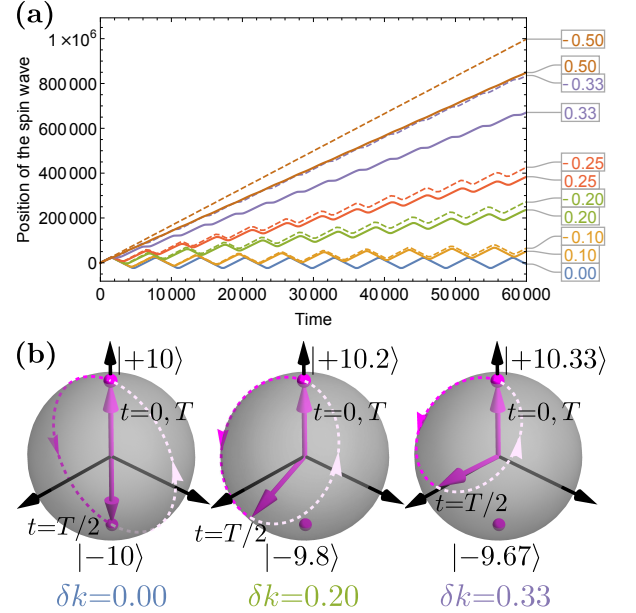


FIG. 2. (a) Time-dependent position of the spin waves with wave vectors $q/2 + \delta k$ after the dc magnonic crystal is switched on at $t = 0$. Different δk [in units of $(2\pi/1000)$] are indicated by the number in the rectangular boxes. Other parameters are $A = 2$, $q = 20 \times (2\pi/1000)$, $\gamma B_0 = 1$, $\Delta = \gamma \Delta B_0 = 0.001$, and $\varphi_s = \varphi_{ac} = 0$. The resonant solution that is closest to the horizontal axis is at $\delta k = 0$. In our plots, the length on the vertical axis is in units of the lattice constant, which is taken to be 1, while the time on the horizontal axis is measured in units $1/\gamma B_0$. The connection between the scales of the spin-wave dynamics in a real physical system and those shown in the figures is discussed in (iii) below. (b) The Bloch-sphere trajectories of the spin waves with three different δk . Here, the trajectories (dashed magenta curves with arrowheads on the surface of the sphere) are plotted only for the first period of the to-and-fro motion; the paths of the second half of the period are indicated by the light color. The intermediate positions of each of the waves are shown by the colored 3D arrows at $t = 0, T/2$, and T , where the period $T = 2\pi/\omega_{\uparrow}(\xi)$.

Spin-wave dynamics in the dc case. In the dc case, by using the ansatz (2) and with the proper initial conditions, one gets a simple analytical solution [23]:

$$S^x(z, t) = \text{Re}[S^+(z, t)] =$$

$$\Delta S \left[(1) \cos\left(\frac{\omega_{\downarrow\uparrow} t}{2}\right) \cos(k_+ z - \Omega t + \varphi_s) + \beta_1(\xi) \sin\left(\frac{\omega_{\downarrow\uparrow} t}{2}\right) \sin(k_+ z - \Omega t + \varphi_s) - \beta_2(\xi) \sin\left(\frac{\omega_{\downarrow\uparrow} t}{2}\right) \sin(k_- z + \Omega t - \varphi_s) \right] \quad (3)$$

with two β functions:

$$\beta_1(\xi) = \frac{\xi}{\sqrt{1+\xi^2}}, \quad \beta_2(\xi) = \frac{1}{\sqrt{1+\xi^2}}. \quad (4)$$

[The solution for $S^y(z, t)$, which has a similar structure, is presented in SM.] In Eq. (3), $\omega_{\downarrow\uparrow} \equiv \omega_{\downarrow\uparrow}(\xi) = (\gamma\Delta B_0)\sqrt{1+\xi^2}$. Here ξ is a dimensionless variable defined as $\xi(\delta k) \equiv \Delta\omega_s(\delta k)/\gamma\Delta B_0$ with $\Delta\omega_s(\delta k) \equiv \omega_s(k_+) - \omega_s(k_-)$; note that $\Delta\omega_s$ depends on δk critically. The parameter ξ describes the level of the energy mismatch of the two spin waves participating in the scattering induced by the dc magnonic crystal; $\Omega \equiv \Omega(\delta k) \equiv [\omega_s(k_+) + \omega_s(k_-)]/2$ is a sort of ‘‘central frequency’’ which depends on δk non-critically. The spin-wave dynamics described by Eq. (3) reminds the one of the Rabi oscillations [23].

In Fig. 2(a) we plot a momentary ‘‘position’’ of the spin wave with wave vector $q/2 + \delta k$ as a function of time for different δk after the dc magnonic crystal is switched on at $t = 0$. [The ‘‘position’’ was determined by tracking numerically the most left zero-crossing point of the imaginary part of the spin-wave solution (2) within a sufficiently large spatial interval.] As one can see from Fig. 2(a), at $\delta k = 0$, the dependence of spin-wave position on time is a zigzag curve around the horizontal axis which indicates the resulting to-and-fro propagation of the spin wave. The period of this zigzag curve is extracted to be $T_{\downarrow\uparrow} \approx 6283 \approx 2\pi/\gamma\Delta B_0$, which indicates that the gap Δ induced by the dc magnonic crystal is equal to $\gamma\Delta B_0$. Moreover, from Fig. 2(a), one may conclude that the to-and-fro motion exists only for a limited interval of δk when $|\delta k| < \delta k_c \approx 0.33$ in units of $(2\pi/1000)$. The critical value δk_c is roughly determined by the criterion $\Delta\omega_s(\delta k_c) = \gamma\Delta B_0$. For the chosen parameters, we get $\Delta\omega_s(0.33) \approx 0.00104$ while $\gamma\Delta B_0 = 0.001$.

Spin-wave dynamics in the ac case. Now, we turn to the ac modulated magnonic crystal. When $\omega_{ac} \neq 0$, the general form of the solution pairs $\mathcal{S}_{p/m}(t)$ and $\mathcal{C}_{p/m}(t)$ is governed by Floquet theorem [30, 31], and the time dependence of the spin-wave dynamics is determined by the quasi-energies of the system. Here we focus only on an important limit when $\omega_{ac} \approx \Delta\omega_s \gg \gamma\Delta B_0$. In this limit, one can implement the rotating wave approximation (RWA) [30]. Under the RWA, we find the approximate solution [23]

$$S^x(z, t) = \text{Re}[S^+(z, t)] \approx \Delta S \left\{ (1) \cos\left(\frac{\omega_R t}{2}\right) \cos\left[k_+ z - \left(\Omega + \frac{\omega_{ac}}{2}\right) t + \varphi_s\right] \right.$$

$$\left. + \beta_1(\tilde{\xi}) \sin\left(\frac{\omega_R t}{2}\right) \sin\left[k_+ z - \left(\Omega + \frac{\omega_{ac}}{2}\right) t + \varphi_s\right] - \beta_2(\tilde{\xi}) \sin\left(\frac{\omega_R t}{2}\right) \sin\left[k_- z + \left(\Omega - \frac{\omega_{ac}}{2}\right) t - \varphi_s - \varphi_{ac}\right] \right\} \quad (5)$$

with $\omega_R \equiv \omega_R(\tilde{\xi}) = (\gamma\Delta B_0/2)\sqrt{1+\tilde{\xi}^2}$, while $S^y(z, t)$ can be found from the imaginary part of $S^+(z, t)$. Here, functions $\beta_1(\tilde{\xi})$ and $\beta_2(\tilde{\xi})$ have the same form as in Eq. (4). However, $\tilde{\xi}$ is defined differently; $\tilde{\xi}(\delta k) \equiv 2[\Delta\omega_s(\delta k) - \omega_{ac}]/\gamma\Delta B_0$. Note that, besides the shift of $\Delta\omega_s$ on the frequency ω_{ac} , there is a factor 2 in $\tilde{\xi}$. The reason why we have $\gamma\Delta B_0/2$ in ω_R (instead of $\gamma\Delta B_0$ as in $\omega_{\downarrow\uparrow}$ for the dc case) is that the ac modulation splits into the rotating and counter-rotating parts, and only the contribution from the rotating component has to be taken into account within the RWA (see SM for more details).

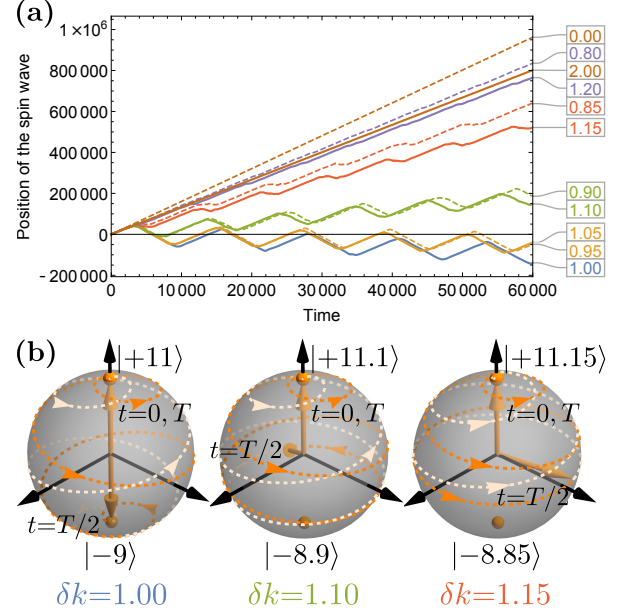


FIG. 3. (a) The time-dependent position of the spin waves with different wave vectors $q/2 + \delta k$ after the ac modulated magnonic crystal with $\omega_{ac} = 0.00316$ is activated at $t = 0$. Other parameters here are the same as in Fig. 2. (b) Trajectories of the spin waves with different δk near the *shifted resonance* on the Bloch sphere. Here, the period $T = 2\pi/\omega_R(\tilde{\xi})$ is different from the dc case.

By properly tuning ω_{ac} , the resonant spin-wave wave vector can be *noticeably* shifted from $q/2$. As one may observe from Fig. 3(a), if ω_{ac} is set to be 0.00316, only the spin waves around $k = 11$ perform the to-and-fro motion accurately enough. For the chosen parameters, namely, $A = 2$ and $q = 20$, one has $\Delta\omega_s(\delta k = 1) \approx 0.00316$ and, therefore, the *shifted resonance* indeed happens at $\tilde{\xi} \approx 0$.

Furthermore, in Fig. 3(a), the period of the zigzag curves around the horizontal axis is doubled as compared with the one in Fig. 2(a). In addition, the width

of the δk intervals at which the to-and-fro motion develops becomes approximately half of the one in the dc case. For example, in Fig. 3(a), the to-and-fro motion can be observed within the interval $10.85 \lesssim k \lesssim 11.15$, while for the dc magnonic crystal presented in Fig. 2(a) it develops when the spin-wave wave vectors are within $9.67 \lesssim k \lesssim 10.33$. All these observations are consistent with our understanding based on the solutions presented by Eqs. (3) and (5).

Bloch-sphere representation. The spin-wave solutions, e.g., the RWA solution in the ac case [cf. Eq. (5) and Eq. (S20) in SM], can be written as

$$\begin{aligned} |\text{SW}\rangle &\equiv S^+(z, t) \\ &\equiv e^{-i\varphi_g(t)} \left\{ \left[\cos\left(\frac{\omega_R t}{2}\right) - i\beta_1(\tilde{\xi}) \sin\left(\frac{\omega_R t}{2}\right) \right] |k\rangle \right. \\ &\quad \left. + \beta_2(\tilde{\xi}) \sin\left(\frac{\omega_R t}{2}\right) e^{i(\omega_{ac} t + \varphi_{ac} - \pi/2)} |k - q\rangle \right\}. \end{aligned} \quad (6)$$

Here, $|k\rangle \equiv (\Delta S)e^{i(k_+ z)}$ and $|k - q\rangle \equiv (\Delta S)e^{i(-k_- z)}$ are two states associated with the wave vectors $k = k_+$ and $k - q = -k_-$. In the second line, the global phase is given with $\varphi_g(t) \equiv \omega_{ac} t/2 + \Omega t - \varphi_s$. [For the dc case, one can obtain the same result as in Eq. (6) by replacing ω_R with $\omega_{\uparrow\downarrow}$ and taking both ω_{ac} and φ_{ac} to be 0.]

The state $|\text{SW}\rangle$ described by Eq. (6) can be represented by a vector, whose ending point is moving on the surface of a Bloch sphere with $|k\rangle$ and $|k - q\rangle$ to be its north and south poles. The motion of the states with different initial wave vectors k on the Bloch spheres, after turning on the dc and ac magnonic crystal, are shown in Figs. 2(b) and 3(b), respectively. As demonstrated by Fig. 2(b), at the resonance (i.e., when $\delta k = 0$), during the first period of the to-and-fro motion, the spin-wave state, which is initially located at the north pole, starts to move to the south pole, and then, after passing the south pole, returns to the north pole. Note that, the spin wave is propagating forward when the state is on the north hemisphere, and vice versa. However, at $\delta k = 0.2$, the trajectory does not pass through the south pole, and its portion below the equator becomes less than the one above the equator. Finally, when $\delta k = \delta k_c \approx 0.33$, the full trajectory is on the north hemisphere only, which indicates the disappearance of the to-and-fro motion.

Figure 3(b), plotted for an ac magnonic crystal with $\omega_{ac} = 0.00316$, shows a more complicated behavior, which includes a non-trivial precession of the states on the Bloch spheres. In the presented case, the resonant spin-wave wave vector is shifted to $k \approx 11$ (and 9).

Discussion and outlook. (i) The dc or ac magnonic crystal created by a metallic meander structure (which is the “hardware” part of the magnonic crystal) with a fixed period $d = 2\pi/q$ can be utilized for the control of the spin waves around $k = q/2$ or where k satisfies the shifted resonance condition $|\omega_s(k) - \omega_s(k - q)| = \omega_{ac}$. As it was presented in Figs. 2 and 3, the spin waves, which are at the resonances (the regular or shifted ones), perform

the to-and-fro motion, while the out-of-resonance spin waves are almost unaffected. The to-and-fro frequency is determined by the band gap, which is controlled by the amplitude of the supplied dc or ac current. The band gap is $\gamma\Delta B_0$ or $\gamma\Delta B_0/2$ (notice the factor 1/2 here) in the dc or ac case. The dc spin-wave dynamics has been demonstrated in Ref. [19] as the oscillatory energy exchange between the wave and its counter-propagating reflection. However, the ac dynamics still remains to be investigated experimentally.

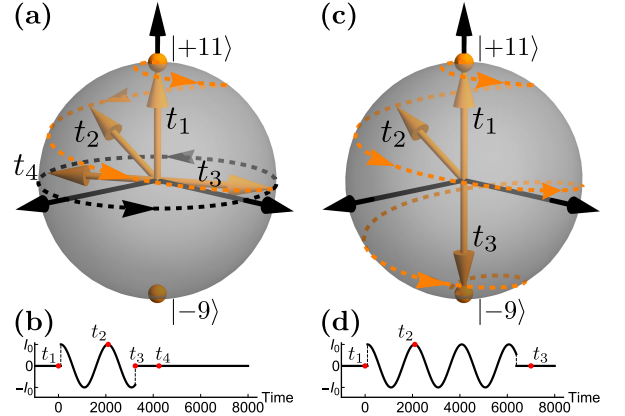


FIG. 4. (a) Motion of the spin wave with the initial wave vector $k = 11$ on the Bloch sphere when sending an ac $\pi/2$ pulse as shown in (b). The dashed orange curve with arrowheads is the trajectory during the activation of the $\pi/2$ pulse, while the dashed black curve on the equator indicates motion after t_3 . (c) Motion when sending π pulse (d). Both pulses are generated at $\omega_{ac} = 0.00316$. The widths of the $\pi/2$ and π pulse are $\pi/2\omega_R$ and π/ω_R , where ω_R is determined by the intensity of the pulse.

(ii) When the spin wave is at the exact shifted resonance (i.e., $\tilde{\xi} = 0$), Eq. (6) is reduced to $|\text{SW}\rangle = e^{-i\varphi_g(t)} \{ \cos[\theta(t)/2] |k\rangle + \sin[\theta(t)/2] e^{i\phi(t)} |k - q\rangle \}$. Here, $\theta(t) \equiv \omega_R t$ and $\phi(t) \equiv \omega_{ac} t + \varphi_{ac} - \pi/2$. This state can be considered as a spin-wave “qubit”, which is characterized by the polar angle $\theta(t)$ and azimuthal angle $\phi(t)$. Recall that $\omega_R(\tilde{\xi} = 0) = \gamma\Delta B_0/2 \propto I_0$; therefore, the time evolution of this “qubit” [i.e., $\theta(t)$ and $\phi(t)$] is fully controlled by the intensity and the ac modulation of the magnonic crystal. Consequently, one can manipulate this spin-wave based macroscopical “qubit” using a properly designed ac pulse. For example, Fig. 4(a) demonstrates that one can bring the state from the north pole to the equator on the Bloch sphere utilizing a $\pi/2$ pulse shown in Fig. 4(b). It is also possible to flip the spin-wave “qubit” by the π pulse, see, e.g., Figs. 4(c) and 4(d), and more discussions in SM. Note that the spin-wave “qubit” controlled by the ac magnonic crystal has a nonzero energy mismatch $\Delta\omega_s = \omega_{ac}$. This leads to a time-dependent $\phi(t)$ and, thereby, opens a way to manipulate the azimuthal angle of this “qubit” and makes all single-qubit operations possible [32].

(iii) Finally, we discuss the feasibility of the proposed

scheme. To make the RWA valid, ω_{ac} has to be much greater than $\gamma\Delta B_0$. In addition, to minimize the higher-order effects from the spin-wave states with wave vectors $k + q$, $k \pm 2q$, \dots , the inequalities of the kind $|\omega_s(k + q) - \omega_s(k) - \omega_{ac}| \gg \gamma\Delta B_0/2$ need to be fulfilled. In particular, one may require $|\omega_s(q) - \omega_s(0) - \omega_{ac}| \gg \gamma\Delta B_0/2$. Let us take the experimental parameters in Ref. [19] as an example. In this measurement, the value of $\gamma\Delta B_0$ was $2\pi \times 11$ MHz, while $|\omega_s(q) - \omega_s(0)|$ was roughly $2\pi \times 100$ MHz. In this case, an ac modulation with ω_{ac} around $2\pi \times 50$ MHz would be suitable for the experimental studies of the shifted resonance. Spin-wave attenuation and decoherence are the two other factors that need to be considered. Let us estimate the operation time required to bring the spin-wave state from the north to the south pole. Using the same value of $\gamma\Delta B_0$, we find this time to be $2\pi/\gamma\Delta B_0 \approx 91$ ns, which is shorter than both lifetime and coherence time of spin waves in YIG (cf. Refs. [8, 9, 14]). In the end, we estimate the length of the device. In practice, the slopes of the curves plotted in Figs. 2(a) and 3(a) are determined by the group velocities of the incident and reflected spin-wave packets, which may vary dramatically for different magnetic material and geometries. In the case of the magnetostatic spin waves studied in Ref. [19], the spin-wave group velocity $|v_g|$ was found to be about 27404 m/s. Such a spin-wave packet would perform to-and-fro motion with

maximum displacement $|v_g| \times 2\pi/\gamma\Delta B_0 \approx 2.5$ mm, and therefore, the meander structure must have a size of at least 2.5 mm in order to confine this bouncing packet. In principle, the operating range of ω_{ac} can be enlarged to a GHz range by fabricating a meander structure with a shorter period d , and the operation time can be further reduced by applying a bigger I_0 .

With the use of the techniques accessible nowadays, the *tunable* ac magnonic crystal can be exploited for controlling spin waves with different wave vectors. One can excite and detect many spin waves with different frequencies in a magnetic sample at the same time through one antenna setup [33]. The tunability of the ac magnonic crystal allows one to use a single hardware (the meander pattern) to simultaneously manipulate multiple spin-wave pairs in one waveguide. Each pair formed by waves with different frequencies is independently operated by a suitable ac pulse that satisfies the *shifted resonance*. As a result, the *tunable* ac magnonic crystal can serve as a new building block of the computing device studied in Ref. [6] and improve its spatial scalability with no compromise on computational time.

Acknowledgements. We appreciate Artem Abanov for reading the manuscript. We thank Karen Michaeli and Alexey Belyanin for discussions. We gratefully acknowledge Dr. Alexander Khitun for the interest in this paper as well as providing us with useful comments on his work.

-
- [1] S. Lloyd, Quantum search without entanglement, *Phys. Rev. A* **61**, 010301(R) (1999).
- [2] P. Knight, Quantum information processing without entanglement, *Science* **287**, 441 (2000).
- [3] D. A. Meyer, Sophisticated quantum search without entanglement, *Phys. Rev. Lett.* **85**, 2014 (2000).
- [4] D. Ferry, R. Akis, and J. Harris, Quantum wave processing, *Superlattices and Microstructures* **30**, 81 (2001).
- [5] A. Patel, Optimal database search: Waves and catalysis, *International Journal of Quantum Information* **04**, 815 (2006).
- [6] M. Balynsky, H. Chiang, D. Gutierrez, A. Kozhevnikov, Y. Filimonov, and A. Khitun, Quantum computing without quantum computers: Database search and data processing using classical wave superposition, *Journal of Applied Physics* **130**, 164903 (2021).
- [7] A. Khitun, R. Ostroumov, and K. L. Wang, Spin-wave utilization in a quantum computer, *Phys. Rev. A* **64**, 062304 (2001).
- [8] A. A. Serga, A. V. Chumak, and B. Hillebrands, YIG magnonics, *Journal of Physics D: Applied Physics* **43**, 264002 (2010).
- [9] M. Collet, O. Gladii, M. Evelt, V. Bessonov, L. Soumah, P. Bortolotti, S. O. Demokritov, Y. Henry, V. Cros, M. Bailleul, *et al.*, Spin-wave propagation in ultra-thin YIG based waveguides, *Applied Physics Letters* **110**, 092408 (2017).
- [10] P. Che, K. Baumgaertl, A. Kúkol'ová, C. Dubs, and D. Grundler, Efficient wavelength conversion of exchange magnons below 100 nm by magnetic coplanar waveguides, *Nature Communications* **11**, 1445 (2020).
- [11] Q. Wang, R. Verba, B. Heinz, M. Schneider, O. Wojewoda, K. Davídková, K. Levchenko, C. Dubs, N. J. Mauser, M. Urbánek, *et al.*, Deeply nonlinear excitation of self-normalised exchange spin waves, [arXiv:2207.01121](https://arxiv.org/abs/2207.01121) (2022).
- [12] A. V. Chumak, V. I. Vasyuchka, A. A. Serga, and B. Hillebrands, Magnon spintronics, *Nature Physics* **11**, 453 (2015).
- [13] G. Csaba, Ádám Papp, and W. Porod, Perspectives of using spin waves for computing and signal processing, *Physics Letters A* **381**, 1471 (2017).
- [14] A. Mahmoud, F. Ciubotaru, F. Vanderveken, A. V. Chumak, S. Hamdioui, C. Adelman, and S. Cotofana, Introduction to spin wave computing, *Journal of Applied Physics* **128**, 161101 (2020).
- [15] P. Pirro, V. I. Vasyuchka, A. A. Serga, and B. Hillebrands, Advances in coherent magnonics, *Nature Reviews Materials* **6**, 1114 (2021).
- [16] H. Yuan, Y. Cao, A. Kamra, R. A. Duine, and P. Yan, Quantum magnonics: When magnon spintronics meets quantum information science, *Physics Reports* **965**, 1 (2022).
- [17] A. V. Chumak, P. Kabos, M. Wu, C. Abert, C. Adelman, A. O. Adeyeye, J. Åkerman, F. G. Aliev, A. Anane, A. Awad, *et al.*, Advances in magnetics roadmap on spin-wave computing, *IEEE Transactions on Magnetics* **58**, 1 (2022).
- [18] A. V. Chumak, V. S. Tiberkevich, A. D. Karenowska, A. A. Serga, J. F. Gregg, A. N. Slavin, and B. Hille-

- brands, All-linear time reversal by a dynamic artificial crystal, *Nature Communications* **1**, 141 (2010).
- [19] A. D. Karenowska, J. F. Gregg, V. S. Tiberkevich, A. N. Slavin, A. V. Chumak, A. A. Serga, and B. Hillebrands, Oscillatory energy exchange between waves coupled by a dynamic artificial crystal, *Phys. Rev. Lett.* **108**, 015505 (2012).
- [20] A. V. Chumak, P. Dhagat, A. Jander, A. A. Serga, and B. Hillebrands, Reverse doppler effect of magnons with negative group velocity scattered from a moving bragg grating, *Phys. Rev. B* **81**, 140404(R) (2010).
- [21] A. V. Chumak, A. A. Serga, and B. Hillebrands, Magnonic crystals for data processing, *Journal of Physics D: Applied Physics* **50**, 244001 (2017).
- [22] A. Liu and A. M. Finkel'stein, Control of spin waves by spatially modulated strain, *Phys. Rev. B* **105**, L020404 (2022).
- [23] See Supplemental Material at <http://link.aps.org/supplemental/10.1103/PhysRevB.107.L180404> for the derivation of the equation of motion, details of the solution, and additional numerical results, which includes Refs. [24–29].
- [24] S. Maekawa, S. O. Valenzuela, E. Saitoh, and T. Kimura, *Spin Current*, Vol. 22 (Oxford University Press, Oxford, 2017).
- [25] M. Holthaus, Floquet engineering with quasienergy bands of periodically driven optical lattices, *Journal of Physics B: Atomic, Molecular and Optical Physics* **49**, 013001 (2016).
- [26] T. Oka and S. Kitamura, Floquet engineering of quantum materials, *Annual Review of Condensed Matter Physics* **10**, 387 (2019).
- [27] C. Cohen-Tannoudji, B. Diu, and F. Laloë, *Quantum Mechanics, Volume 1: Basic Concepts, Tools, and Applications* (Wiley-VCH, Hoboken, 2020).
- [28] Wolfram Research, NDSolve, online <https://reference.wolfram.com/language/ref/NDSolve.html> (Accessed: 29-May-2022).
- [29] P. B. Visscher, A fast explicit algorithm for the time-dependent Schrödinger equation, *Computers in Physics* **5**, 596 (1991).
- [30] M. Grifoni and P. Hänggi, Driven quantum tunneling, *Physics Reports* **304**, 229 (1998).
- [31] M. Bukov, L. D'Alessio, and A. Polkovnikov, Universal high-frequency behavior of periodically driven systems: from dynamical stabilization to Floquet engineering, *Advances in Physics* **64**, 139 (2015).
- [32] M. A. Nielsen and I. Chuang, *Quantum Computation and Quantum Information* (Cambridge University Press, Cambridge, 2010).
- [33] A. Khitun (private communication).